Epitaxial growth of strained Mn5Ge3 nanoislands on Ge(001)

Sion F. Olive Mendez, Lisa A. Michez, Aurelie Spiesser, and Vinh LeThanh

Abstract

We report on the epitaxial growth of Mn5Ge3 on Ge(001) by molecular beam epitaxy using solid phase epitaxy method. Mn5Ge3 grows as nanoislands, which are randomly distributed over the substrate surface. Select area electron diffraction analysis was used to determine the epitaxial relationship Mn5Ge3(001)[110]//Ge(001)[110], as well as to detect an induced tensile strain along [110] Mn5Ge3 direction to fit the Ge lattice, while the observation of Moiré patterns indicates a complete relaxation along the $[1\bar{1}0]$ direction. In-plane and out-of-plane M(H) loops were obtained at 200 K using a vibrating sample magnetometer, it was found that the easy axis of magnetization is perpendicular to the substrate surface and that the crystal magnetic anisotropy is K1 = 9.27 × 105 erg cm−3. The enhancement of the Curie temperature of the nanoislands ∼340 K, which is higher than 296 K of the bulk Mn5Ge3, is attributed to the induced strains.

1 Introduction

One of the major challenges in developing spintronic devices concerns a reliable injection and detection of spin polarized currents. An efficient method is the use of a ferromagnetic material, which can be directly grown on a semiconducting substrate [1]. It has recently been reported the achievement of spin injection on n-type Ge using epitaxial Mn5Ge3 thin films [2] or nanowires [3, 4]. Polarized

electrons, from the intermetallic compound, pass through a Schottky barrier at the Mn5Ge3/Ge interface [5], where the width of the barrier depends on the crystal quality of the interface [6]. Mn5Ge3 can be grown on Ge(111) substrates by solid phase epitaxy (SPE) method consisting of Mn deposition at room temperature followed by thermal annealing at ~450 °C to promote diffusion between the deposited layer and the Ge atoms from the substrate, even if Mn5Ge3 is not the most stable phase on the Ge–Mn phase diagram [7, 8]. Mn5Ge3 has a hexagonal D88 crystal structure (space group 193 or P63/mcm) with unit cell parameters a = 7.184 Å and c = 5.053 Å. The mismatch between the (0001) basal plane of Mn5Ge3 and the surface lattice parameter of Ge(111) is 3.7%. The epitaxial relationship for thin films grown on Ge(111) is Mn5Ge3(001)[100]//Ge(111)$[1\bar{1}0]$ where the film exhibits a $(\sqrt{3} \times \sqrt{3})$R30° surface reconstruction. The strain is relaxed within a thickness of 1 nm confirmed by reflection high-energy electron diffraction (RHEED) [9], however, observations using high-resolution transmission electronic microscopy did not reveal the presence of misfit dislocations.

The Curie temperature (TC) of Mn5Ge3 thin films is 296 K, which can be enhanced by carbon doping up to 450 K [10, 11]. It has been recently reported that strained Mn5Ge3 thin films grown on GaSb(001) and GaAs(001) substrates, lead to an enhancement of Curie temperature up to 320 and 350 K, respectively [12]. The easy magnetization axis for bulk material lies along the c axis of the crystal structure; for thin films with thickness under 10 nm, the easy magnetization axis lies on the film plane [13] whereas for thicker films there is a competition between magnetostatic energy and magnetocrystalline energy [14], which makes that the easy

magnetization axis turns progressively out of the in-plane configuration. The crystal anisotropy constant of bulk-Mn5Ge3 is K1 = 3 × 105 erg cm−3at room temperature [15]. Zeng et al. [16] reported that for epitaxial thin films grown on Ge(111), K1at 5 K is 2.66 × 106 erg cm−3.

Despite the work devoted to the study of Mn5Ge3 thin films grown on Ge(111), the integration of Mn5Ge3 with high TC into the complementary metal-oxide-semiconductor (CMOS) Si-based technology requires the knowledge to successfully grow such ferromagnetic material in Ge(001) substrates, which in turn is easy to epitaxially grow on Si(001). Previous reports of the growth of Mn5Ge3 on Ge(001) leads with the growth of nanoislands [17] or self-assembled nanocrystals embedded on Ge1−xMnxepilayers [18-20], however, there is a lack on the study of the magnetic properties. In this paper, we report the epitaxial growth Mn5Ge3 nanoislands on Ge(001) with high TC, which is attributed to the tensile strain induced by the substrate. We present a detailed study of the structural characterization and the modification of the magnetic properties compared to those obtained in epitaxial films on Ge(111) substrates.

2 Experimental methods

The Mn5Ge3 nanoislands were grown in a molecular beam epitaxy (MBE) system with a base pressure of 1 × 10−10 Torr. The chamber is equipped with a reflection high-energy electron diffraction (RHEED) system to control the Ge surface preparation and crystallization of Mn5Ge3 nano-islands. Germanium substrates were cleaned with wet chemical cleaning process followed by in situ thermal annealing at 750 °C and the growth of a Ge buffer layer in order to obtain an

atomically clean and flat Ge surface exhibiting a 2 × 1 reconstructed surface. Manganese deposition was performed using a Knudsen cell with a growth rate of 0.3 nm min−1. Six atomic mono-layers of Mn (~0.9 nm) were deposited on Ge(001) substrates at room temperature followed by thermal annealing at 650 °C to activate diffusion between Ge and Mn (SPE method). High resolution-transmission electron microscopy (HR-TEM) micrographs and selected area electron diffraction (SAED) patterns were obtained using a JEOL 3010 FX microscope operating at 300 kV, with samples prepared in cross-section and in plane-view geometry. In-plane and out-of-plane magnetic M(H) loops were obtained at 200 K using a vibrating sample magnetometer (VSM) and saturation magnetization depending on the temperature Ms(T) curve was obtained to determine TC.

3 Results and discussion

The RHEED patterns of the Ge(001) substrate along the $[1\bar{1}0]$ and [100] directions are presented in Fig. 1a and b, respectively, showing a clear 2 × 1 surface reconstruction corresponding to an atomically clean and flat surface. Over this surface the Mn deposition was carried out at room temperature. The ½ order streaks disappear and one can only observe week 1 × 1 streaks as the Mn coverage is homogeneously distributed all over the substrate. After annealing at 650 °C, diffraction spots are observed along the same azimuths of the substrate and are shown in Fig. 1c and d. The 3-dimensional feature (i.e., spots on the RHEED pattern) only appears when the electron beam passes through some formed islands on a rough surface. For comparison, in Fig. 1e and f are shown the RHEED patterns obtained after the growth of a continuous Mn5Ge3 thin film on Ge(111). One can

observe that the 3D-spots have a correspondence with the 1 × 1 and the ⅓ and ⅔ order streaks

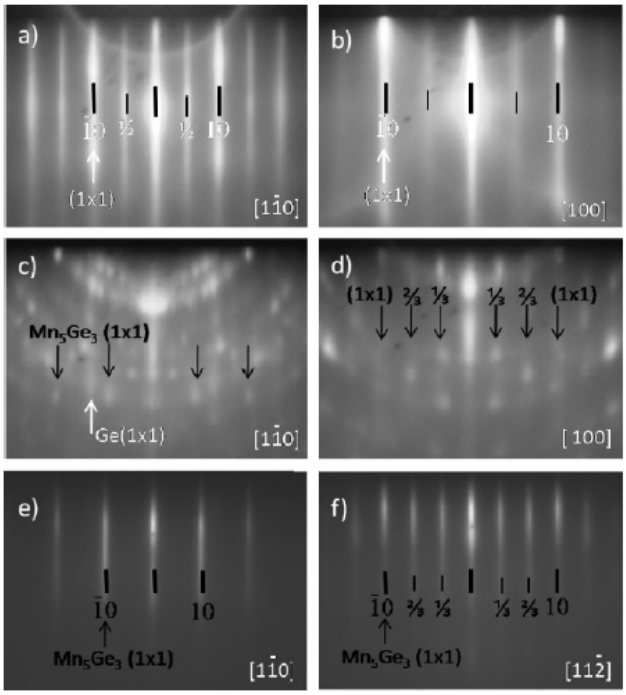

Figure 1 RHEED patterns of reconstructed Ge(001) surface along (a) ½1$\bar{1}$0] and (b) [100] directions. After annealing at 650 8C, 3-dimensional spots can be observed in (c) and (d). For comparison purposes, there is also shown the RHEED pattern of a reconstructed $(\sqrt{3} \times \sqrt{3})$R308 surface of Mn_5Ge_3 grown on Ge(111) along(e) [1$\bar{1}$0] and (f) [11$\bar{2}$] directions of the substrate. One can observe a clear correspondence of the 1 × 1 streaks and the $^{1}3$ and $^{2}3$ order streaks of Mn_5Ge_3 on both substrates.

of the $(\sqrt{3} \times \sqrt{3})$R30° surface reconstruction of Mn5Ge3. The obtained RHEED patterns can be, without a mistaken interpretation, attributed to Mn5Ge3. Other phases as Mn11Ge8 or Mn5Ge3 are obtained during the synthesis of diluted magnetic semiconductors at temperatures ranging from 70 to 120 °C [21].

An atomic force microscopy (AFM) micrograph of the sample surface is shown in Fig. 2 illustrating three main groups of different sizes of Mn_5Ge_3 nanoislands randomly distributed over the surface. The biggest islands belong to group A and are characterized by an average size of ~78 nm and a

population of 2.45 islands μm^{-2}; the nano-islands of group B have an average size of ~30 nm and a density of 5 islands μm^{-2}. The third group C is constituted of islands with a very small diameter (<20 nm) and a density twice higher than that of B islands. The mean separation between the islands of groups A and B is 318 nm. The inset of Fig. 2 shows the histogram of the island size distribution. During heating, the continuous Mn film is fragmented and small Mn clusters may diffuse on the surface creating agglomerates by coalescence. Larger agglomerates do not have enough energy to diffuse and then atomic diffusion of Mn and Ge leads to a chemical reaction to produce the Mn_5Ge_3 nanoislands. The authors have shown in a previous report

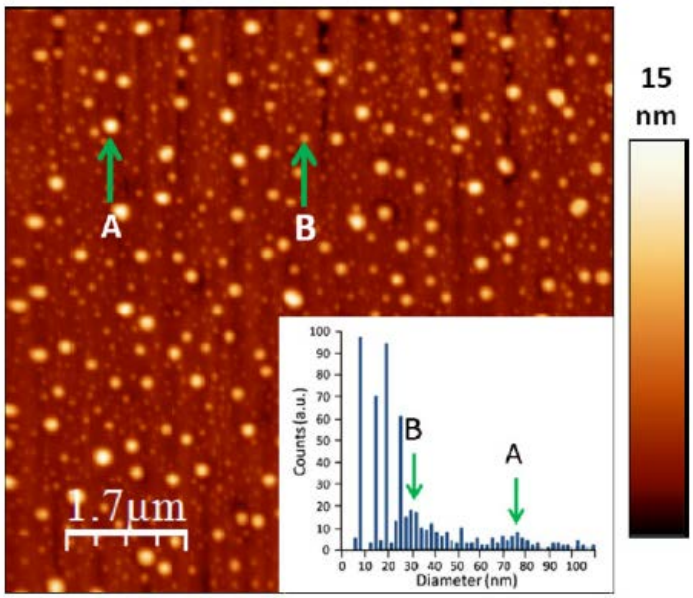

Figure 2 AFM micrograph of the sample surface with the Mn_5Ge_3 nanoislands. Island groups A and B correspond to the predominant sizes as shown on the histogram in the inset.

that Mn_5Ge_3 films grown on Ge(111) are stable up to 850 °C, after that the film split leading to the formation of nanoislands, with a similar size and distribution than the ones reported here, however the Mn_5Ge_3/Ge interface remains at the same level than the Ge surface [**7**].

Figure 3a shows a cross-section TEM micrograph of a nanoisland with a diameter ~100 nm. Remarkably, one can see that Mn5Ge3/Ge interface is not limited at the substrate surface, instead, about 2/3 of the nanoisland height is submerged under the sample surface and only 1/3 is exposed above it, which offers a comparison between the growth of Mn5Ge3 on Ge(001) and Ge(111). In the latest case, we have the agreement of the hexagonal symmetry of both the Mn5Ge3(001) basal plane and the Ge(111) surface. Similar growth has been observed on in-plane nanowires of several metals (Ti, Mn, Fe, Co, Ni, and Pt) on different facets of Si substrates [22], a particular case of epitaxial growth known as endotaxy, where the metal/substrate interface is found under the surface level of the substrate. According with the growth mechanisms of thin films, a continuous thin film requires that $\gamma_s > \gamma_{int} + \gamma_f$, where γ represents the surface energy of the f (film), s (substrate), and int (interface). In our case, the 3-dimensional growth is attributed to a change in the previous equation to $\gamma_s \geq \gamma_{int} + \gamma_f$ through a modification of γ_{int}. The effect of the surface free energies of the {001} and {111} facets of Ge, which are 1710 and 1300 erg cm^{-2}, respectively [**23**], may play an important role in the nanoisland growth, as it will be shown later. The value of γ_{int} may suffer a change as the cell of Mn_5Ge_3 has to compensate the lattice mismatch and also the difference of the substrate/film symmetry (hexagon/square), then the nanoisland-like growth should

be a mechanism to reduce the total energy of the system. Furthermore, using the Wulff–Kaichev's theorem [**24**] $\gamma_i/h_i = (\gamma_{int} - \gamma_s)/h_{int}$,

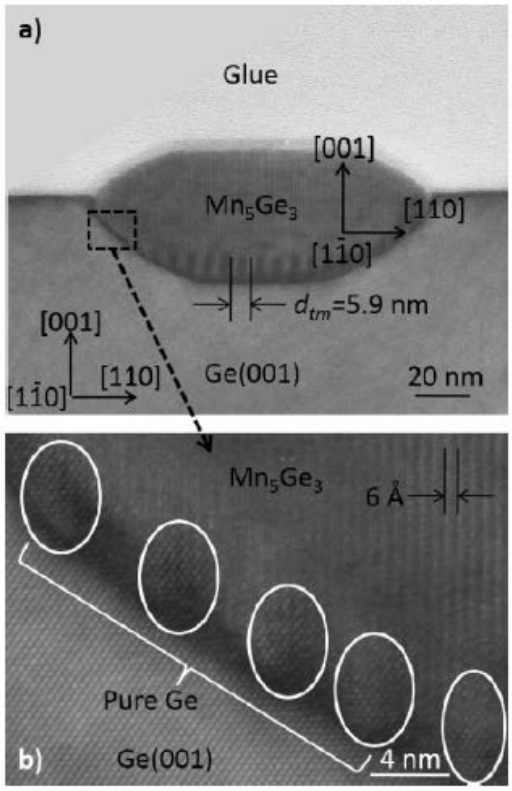

Figure 3 (a) TEM cross-section micrograph of a nanoisland. The Mn_5Ge_3/Ge interface penetrates into the substrate due to the higher surface free energy of the Ge(001) surface compared to that of the {111} facet (b) Mn_5Ge_3/Ge(001) side interface showing the vertical Mn diffusion path.

where hint is the distance between the center of the crystal to the interface (i.e., the position at which is found the surface of the substrate) we can make a rough estimation of γint. For our nanoislands hint is negative as the center of the nanocrystal is found under the z = 0 position of the Ge surface, then $\gamma_{int} - \gamma_s$ should be less than 0 to fit the equation. Then we obtain $\gamma_{int} < \gamma_s$ (were γs = 1710 erg/cm2); making the same analysis for a continuous thin film, we found that $\gamma_{int} > \gamma_s$ (here γs = 1300 erg cm−2) then γint can get different values in the range 1300–1710 erg cm−2 for the Mn5Ge3 growth on either of the Ge substrates. From the

shape of the nanocrystal and using the criteria of the Wulff construction [25], we can relate the values of the surface free energy of each exposed facet depending on the distance facet to the center of the crystal. However, the determination of the exact values requires further theoretical calculations. In Fig. 3b, is shown a HR-TEM micrograph of a section of the interface, showing alternating Ge zones (which are Mn-free) separated by Mn5Ge3 zones formed by Mn diffusion. The existence of Mn-free vertical zones suggest that first Mn is segregated to form clusters on the Ge(001) surface and then the diffusion process occurs between Mn and Ge, which react to produce Mn5Ge3. At this point no relaxation mechanism, as dislocations, were observed in the cross-sectional HR-TEM micrographs. However, it can be stated that the zones containing the Ge inclusions may act as some relaxation mechanism limited to the external circular zone of the nanoisland (see also the bright-shell zone in Fig. 4b). Further HR-TEM investigation of the sample prepared in plane-view geometry offered a global view of the nanoislands scattered over the substrate (Fig. 4a). The observed Moiré patterns in Fig. 4b and at the bottom of the nanoisland in Fig. 3b with a separation of 5.9 nm appear due to the superposition of two crystal structures with a different but very close lattice parameter. The interatomic separation along the $[1\bar{1}0]$ direction of the Ge substrate is 2 Å. We use the equation, which links the lattice parameters with the Moiré pattern length:

$$d_M = \frac{d_2 d_1}{d_1 - d_2},$$

where dM is the Moiré periodicity and d1 and d2 are the lattice parameters of the superposed lattices with d1 > d2. By fixing d2 = 2 Å we obtain that d1 = 2.07 Å, which exactly match ⅓ of the Mn5Ge3 alattice parameter along the $[1\bar{1}0]$ direction

(i.e., $3 \times 2.07 \approx 6.22 = 7.184 \cos 30°$). The lattice mismatch along this direction is 3.69%, however, the material remains relaxed. The inset in Fig. 4b shows a HR-TEM micrograph of one nanoisland, where Moiré patterns have higher contrast and reveal a fine structure belonging to Mn5Ge3 interatomic separation along the $[1\bar{1}0]$ direction where the interatomic distance is 6.22 Å.

Figure 4c shows the in-plane SAED pattern of the nanoisland shown in Fig. 4b. The indexation of the spots reveals that the epitaxial relationship of the nanoislands with the substrate is: Mn5Ge3(001)[110]//Ge(001)[110]. It can also be noted how the (330) and $(\bar{3}\bar{3}0)$ reflects of Mn5Ge3 perfectly match the (220) and $(\bar{2}\bar{2}0)$ reflects of Ge. This observation indicates that Mn5Ge3 nanoislands remain under tensile strain along the [110]Ge direction inducing a deformation on the nanoislands of $\Delta[110] = 10.25\%$. This deformation include a reduction on the angle between the a and b axis from 120° to 112.33° leading to a monoclinic crystal structure. Figure 4d shows a simulated electron diffraction pattern of relaxed Mn5Ge3 (black open circles) superposed over the Ge diffraction pattern (red filled circles) both along the [001] zone axis. The two top black arrows in panels (c) and (d) indicate how the (330) and the (660) reflects of Mn5Ge3 will appear in the SAED pattern if the nanoislands were relaxed along the [110] direction. One can also note that three reciprocal cells of Mn5Ge3 perfectly match with the Ge reflects along this direction. On the other hand, the relaxation along the $[1\bar{1}0]$ direction can also be evidenced in the SAED pattern as non-concentric reflects are found (encircled in green) and compared to that of panel (d) through the green arrow.

A top-view diagram depicting the epitaxial relationship of the

Mn5Ge3 nanoislands with the substrate is shown in Fig. 5, where the Mn5Ge3 unit cell is already tuned into the monoclinic structure. It is shown that along the $[1\bar{1}0]$ direction of either the substrate or the Mn5Ge3 crystal structure, two Mn5Ge3 unit cells are required to roughly fit three Ge cells. The nanoislands remain relaxed along this direction, showing the lattice mismatch indicated by blue circles. The picture changes if we look to the perpendicular direction, where the islands acquire exactly the lattice from the substrate; in the diagram, the blue lines are a guide for the eye to indicate the lattice match. It is possible that compressive deformation may occurs along the c axis to compensate this high deformation. Additionally, we have succeed on the growth of a epitaxial Mn5Ge3 thin films on Ge(001) using co-deposition of pure Mn and Ge. The film exhibits three epitaxial relationships, where each monocrystalline region has an average size of ~80 nm, it is possible

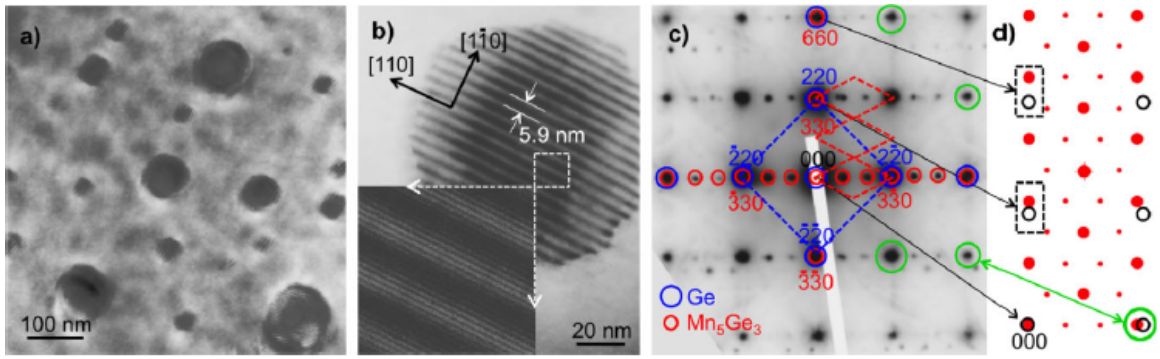

Figure 4 (a) TEM plane-view micrograph of Mn_5Ge_3 nanoislands. (b) HR-TEM of a nanoisland with Moiré fringes along $\frac{1}{2}1\bar{1}0]_{Ge}$ with periodicity of 5.9 nm, the inset shows the Moiré patterns and relaxed Mn_5Ge_3 rows. (c) SAED pattern from the nanoisland in panels (b) and (d) simulated electron diffraction pattern along [001] zone axis of relaxed Mn_5Ge_3 structure (open black circles) and Ge substrate (full red circles). The black arrows provide a comparison between tensile to relaxed material along [110] direction. The green circles and arrow show how the material is relaxed along $\frac{1}{2}1\bar{1}0]$ direction.

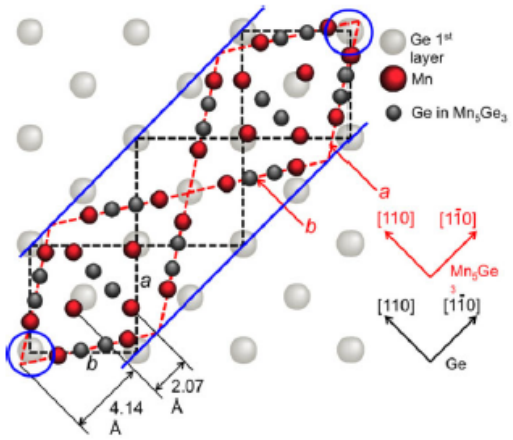

Figure 5 Diagram depicting the epitaxial relationship of hexago-nal Mn_5Ge_3 which is relaxed along ½1$\bar{1}$0] direction (blue circles) and strained along [110] direction, fitting the Ge lattice parameter (blue lines).

that Mn5Ge3 may support the described tensile deformation up to a given extension and that additional epitaxial relationships act as a mechanism to overcome the substrate induced strain. These results will be published later. Similar growth of strained films has been reported on the growth of Mn5Ge3 on GaSb(001) and GaAs(001) substrates [12].

The in-plane and out-of-plane magnetic M(H) loops obtained at 200 K are shown in Fig. 6a. For each loop, the diamagnetic component arising from the substrate was mathematically subtracted until the slope of the curve at high field is zero; the subtracted quantity match with the measured diamagnetic susceptibility of a Ge bare substrate. The out-of-plane measurement is an almost square-like loop with hysteresis exhibiting a clear remanence and coercivity demonstrating that magnetic domains (or monodomains) are well aligned along c axis. An opposite behavior is obtained on the in-plane measurement, where an anhysteretic loop is obtained due to a measurement performed along a hard magnetization axis. Saturation magnetization Ms is obtained at a field $\mu_0 H_a = 0.2$ T (2000 Oe). Both measurements demonstrate that the easy

magnetization axis is perpendicular to the sample surface. The difference on the saturation magnetization values of both measurements at high magnetic fields is attributed to the demagnetizing factors for an ellipsoid; we can roughly make an approximation with a = b and c/a = 0.33, which produce the demagnetizing factors [26]: in-plane N = 0.1820 and out-of-plane N = 0.688. The net magnetic moment of the sample will be then $19.33 \pm 0.72 \times 10{-}6$ emu, corresponding to a saturation magnetization $Ms = 927 \pm 120$ emu $cm{-}3$ which is very close to $Ms = 1200 \pm 150$ emu $cm{-}3$ for epitaxial Mn5Ge3/Ge(111) thin films. The magnetic moment per Mn atom obtained from the out-of-plane M(H) loop is 1.13 ± 0.14 μB that increases to 2.27 ± 0.3 μB if we consider the effect of shape anisotropy. Using the expression Ms = 2K1/μ0Ha for the magnetocrystalline anisotropy for a material with a

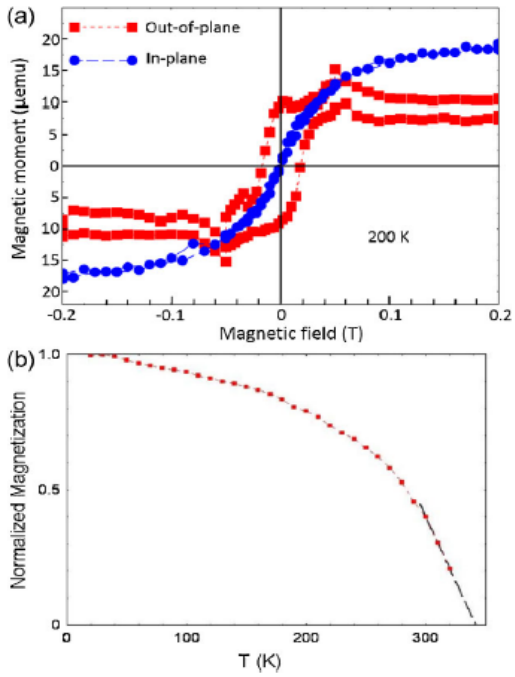

Figure 6 (a) In-plane and out-of-plane M(H) measurements after subtraction of the diamagnetic component from the substrate.(b) Saturation magnetization dependence of the temperature of the Mn_5Ge_3 nanoislands showing a T_C ~340 K.

hexagonal crystal structure, we found that K1 at 200 K for the nanoislands is 9.27 × 105 erg cm−3. From the saturation magnetization dependence on the temperature shown in Fig. 6b, we observe that by extrapolation of the curve, TC of nano-islands is ∼340 K, which is higher than 296 K obtained on thin films. This enhancement of TC can be attributed to the tensile-compressive strain, which may change the interatomic Mn–Mn distances modifying the value of the exchange integral. Similar TCenhancement (350 K) has been reported on strained Mn5Ge3 thin films on GaAs(001) substrate [12]. Also, it has been theoretically calculated that an increase on the cell volume produces a non-collinear alignment of the magnetic moment of the Mn atoms, together with a high spin configuration [27]. As expected, the increase on the volume of the Mn5Ge3 cell on the nanoislands should be accompanied by a higher thermal stability of the Mn magnetic moments.

4 Conclusions

We have shown the feasibility of epitaxial growth of Mn5Ge3 on Ge(001) resulting in formation of Mn5Ge3 nano-islands. The obtained epitaxial relationship is Mn5Ge3(001)[110]//Ge(001)[110]. From the SAED patterns, we find that the nanoislands exist under strain to fit the square symmetry of the substrate, the deformation along the [110] direction is 10.25% while the material remain relaxed along the $[1\bar{1}0]$ direction producing Moire patterns. The induced deformation is accompanied with a switch from the basal hexagonal structure to a monoclinic structure with an angle of 112.62°. The net magnetization of the nanoislands is Ms = 927 ± 120 emu cm−3 and the easy magnetization axis is parallel to the c axis, which in turn is perpendicular to the substrate surface. The anisotropy constant at

200 K is K1 = 9.27 × 105 erg cm−3. An increase of the TC up to ∼340 K is attributed to an expansion on the cell volume, which leads to a modification of the direct exchange interaction between Mn atoms.

Reference

[1] H. Ikeya, Y. Takahashi, N. Inaba, F. Kirino, M. Ohtake, and M. Futamoto, J. Phys. Conf. Ser. 266, 012116 (2011).

[2] A. Spiesser, H. Saito, R. Jansen, S. Yuasa, and K. Ando, Phys. Rev. B 90, 205213 (2014).

[3] J. Tang, C.-Y. Wang, M.-H. Hung, X. Jiang, L.-T. Chang, L. He, P.-H. Liu, H.-J. Yang, H.-Y. Tuan, L.-J. Chen, and K. L. Wang, Nano Lett. 6(6), 5710 (2012).

[4] J. Tang C.-Y. Wang, L.-J. Chen, and K. L. Wang, 12th IEEE Conference on Nanotechnology (IEEE-NANO) (2012).

[5] R. Jansen, A. Spiesser, H. Saito, and S. Yuasa, cond-mat.mes-hall arXiv:1410.3994v2 (2014).

[6] A. Sellai, A. Mesli, M. Petit, V. Le Thanh, D. Taylor, and M. Henini, Semicond. Sci. Technol. 27, 035014 (2012).

[7] C. Zeng, S. C. Erwin, L. C. Feldman, A. P. Li, R. Jin, Y. Song, J. R. Thompson, and H. H. Weitering, Appl. Phys. Lett. 83, 5002 (2003).

[8] S. Olive-Mendez, A. Spiesser, L. A. Michez, V. Le Thanh, A. Glachant, J. Derrien, T. Devillers, A. Barski, and M. Jamet, Thin Solid Films 517, 191 (2008).

[9] A. Spiesser, S. F. Olive-Mendez, M.-T. Dau, L. A. Michez, A. Watanabe, V. Le Thanh, A. Glachant, J. Derrien, A. Barski, and M. Jamet, Thin Solid

Films 518, S113 (2010).

[10] M. Petit, M. T. Dau, G. Monier, L. Michez, X. Barre, A. Spiesser, V. Le Thanh, A. Glachant, C. Coudreau, L. Bideux, and C. Robert-Goumet, Phys. Status Solidi C 9(6), 1 (2012).

[11] A. Spiesser, V. Le Thanh, S. Bertaina, and L. A. Michez, Appl. Phys. Lett. 99, 121904 (2011).

[12] D. D. Dang, O. Dorj, V. Le Thanh, C. H. Soon, and C. Sunglae, J. Appl. Phys. 114, 073906 (2013).

[13] V. Le Thanh, A. Spiesser, M.-T. Dau, S. F. Olive-Mendez, L. A. Michez, and M. Petit, Adv. Nature Sci.: Nanosci. Nanotechnol. 4, 043002 (2013).

[14] A. Spiesser, F. Virot, L.-A. Michez, R. Hayn, S. Bertaina, L. Favre, M. Petit, and V. Le Thanh, Phys. Rev. B 86, 035211 (2012).

[15] Y. K. Tawara and K. Sato, J. Phys. Soc. Jpn. 18(6), 773 (1963).

[16] C. Zeng, S. C. Erwin, L. C. Feldman, A. P. Li, R. Jin, Y. Song, J. R. Thompson, and H. H. Weitering, Appl. Phys. Lett. 83 24 5002 (2003).

[17] H. Kim, G.-E. Jung, J.-H. Lim, K. H. Chung, S.-J. Kahng, W.-J. Son, and S. Han, Nanotechnology 19, 025707 (2008).

[18] R. T. Lechner, V. Hol□y, S. Ahlers, D. Bougeard, J. Stangl, A. Trampert, A. Navarro-Quezada, and G. Bauer, Appl. Phys. Lett. 95, 023102 (2009).

[19] J. Zou, Y. Wang, F. Xiu, K. L. Wang, and A. P. Jacob, Appl. Phys. Lett. 96, 051905 (2010).

[20] Y. Wang, J. Zou, Z. Zhao, X. Han, X. Zhou, and K. L. Wang,

J. Appl. Phys. 103, 066104 (2008).

[21] Y. Wang, J. Zou, Z. Zhao, X. Han, X. Zhou, and K. L. Wang, Appl. Phys. Lett. 92, 101913 (2008).

[22] P. A. Bennett, Z. He, D. J. Smith, and F. M. Ross, Thin Solid Films 519, 8434 (2011).

[23] A. A. Stekolnikov, J. Furthm€uller, and F. Bechstedt, Phys. Rev. B 65, 115318 (2002).

[24] P. M€uller and R. Kern, Surf. Sci. 457, 229 (2000).

[25] G. Wulff and Z. Kristallogr, Mineral 34, 449 (1901).

[26] J. A. Osborn, Phys. Rev. 67(11), 351 (1945).

[27] A. Stroppa and M. Peressi, Mater. Sci. Semicond. Process. 9, 841 (2006).